Piezoresponse force microscopy behaviour of $Bi_4Ti_3O_{12}$ ceramics with various excess bismuth

Ederson C. Aguiar[1], Alexandre Z. Simões[2,*], Francisco Moura[3], Mario Cilense[1], Elson Longo[1], Jose A. Varela[1]

[1]*São Paulo State University, UNESP, Chemistry Institute, Department of Chemistry-Physics, P.O Box 355, 14800-900, Araraquara, São Paulo, Brazil*

[2]*São Paulo State University, UNESP, Engineering Faculty, P.O Box 355, 12516-410, Guaratinguetá, São Paulo, Brazil*

[3]*Federal University of Itajubá- Unifei - Campus Itabira, Rua São Paulo 377, Bairro Amazonas, P.O. Box 355, 35900-37, Itabira, Minas Gerais, Brazil*

Received 19 November 2010; received in revised form 21 January 2011; accepted 14 February 2011

Abstract

Bismuth titanate ($Bi_4Ti_3O_{12}$ - BIT) ceramics derived from different amounts of excess Bi_2O_3 were prepared using the polymeric precursor method. In spite of excess bismuth, single phase ceramics were obtained with a controlled microstructure. Raman analysis evidenced typical vibrational bands of the BIT phase. UV-vis spectra indicated that excess Bi_2O_3 causes a reduction in defects in the BIT lattice due to the suppression of oxygen vacancies located at the octahedral BO_6^- ion. The microstructure and electrical properties are strongly dependent on the excess Bi_2O_3. Appropriate initial Bi_2O_3 excess reduces the leakage current and loss tangent and thereby improves the polarization of BIT ceramics. Rietveld analyses confirmed that the powders crystallize in an orthorhombic structure with a space group of Fmmm at room temperature. The polarization reversal was investigated by applying ac voltage through a conductive tip during the area scanning and was investigated by piezoresponse force microscopy (PFM).

Keywords*: bismuth titanate, chemical synthesis, annealing, dielectric properties*

I. Introduction

Recently, compounds with an Aurivillius structure have been investigated, such as: BBT (barium bismuth tantalate), SBN (strontium bismuth niobate), SBT (strontium bismuth titanate), BBN (barium bismuth niobate) and BIT (bismuth titanate). BIT is a promising ferroelectric material which is used in non-volatile random access memories [1,2]. $Bi_4Ti_3O_{12}$ has interesting properties: high Curie temperature, high remanent polarization and low coercive field. These properties are due to the Bi_2O_2 layers separated by perovskite planes of type $Bi_2Ti_3O_{10}$ in the orthorhombic structure. The crystal structures of BLSFs (bismuth-layer-structured ferroelectrics) are generally formulated as $(Bi_2O_2)^{2+}(A_{m-1}B_mO_{3m+1})^{2-}$ where A represents mono-, di-, or trivalent ions, B represents tetra-, penta-, or hexavalent ions with appropriate size and valence, and m is the number of BO_6 octahedra in the pseudoperovskite blocks (m = 1, 2, 3, 4, and 5). The perovskite blocks, $(A_{m-1}B_mO_{3m+1})^{2-}$, are sandwiched between bismuth oxide layers, $(Bi_2O_2)^{2+}$ along the *c*-axis [3]. The electric and dielectric properties of the blocks have been improved by the addition of excess bismuth. These studies revealed that when the value of the excess Bi content in precursor sols is 10 mol% the best polarization-electric field, capacitance-voltage and dielectric characteristics were attained. Also, the addition of a 3 mol% excess of Bi_2O_3 resulted in a drastic decrease in the leakage current [4,5]. The excess Bi_2O_3 in SBT indicated that the phase-transition and ferroelectric properties such as spontaneous polarization (P_s) showed a dependence on the Bi content. The ferroelectric Curie temperature T_c decreased with an

* Corresponding author: tel: +55 12 3123 2765
fax: +55 12 3123 2800, e-mail: *alezipo@yahoo.com*

increasing in the Bi content and the P_s was maximized when 2–3 mol% excess of Bi_2O_3 was added [6]. In other work, addition of 10 mol% Bi excess in $BaBi_2Ta_2O_9$ increased the dielectric permittivity with decreasing *tan δ* while improve ferroelectric properties [7]. In another experiment, bismuth titanate with an excess of 5 wt.% Bi was added to the stoichiometic mixture aiming to minimize the bismuth loss during the thermal treatment. Without the addition of bismuth, pure phase could not be obtained [8].

Due to this high transition temperature, BIT ceramics are good candidates for high temperature piezoelectric applications. The main problem concerning their practical application as piezoelectrics is the relatively low electrical resistivity. The electrical conductivity in BIT is highly anisotropic, with the maximum value in the same plane of the vector polarization. As a consequence, BIT ceramics are very difficult to pole. Thus the reduction of electrical conductivity is one of the main goals the worldwide investigations of BIT [9].

The BIT-based ceramics microstructure reflects the structural anisotropy showing larger platelets-like grains growing preferentially in the *a–b* plane. The electrical response of these materials is strongly dependent on the microstructure [10,11]. The conventional ceramic route synthesis leads to undesireable phases due to volatilization of Bi_2O_3 at elevated temperatures [12]. The formation of secondary phases can be avoided by decreasing the calcination temperature or using wet-chemistry based methods. By using chemical methods, (e.g. coprecipitation, sol-gel, hydrothermal and the Pechini method [13]), it is possible to control the morphology and chemical composition of the powders. Due to the easy volatilization of Bi_2O_3 in the fabrication process, initial excess bismuth can strongly affect the structure and physical properties of the $Bi_4Ti_3O_{12}$-based materials. Kim and Kim [14] studied the effect of excess bismuth on the crystallization of BLT thin film prepared by MOD. Lin *et al*. [15] studied the role of excess bismuth on the orientation and ferroelectricity of BLT film by CSD. However, limited research has been conducted related to the microscopic effect that excess bismuth can cause in $Bi_4Ti_3O_{12}$-based ceramics. The aim of this paper is to examine the effects of initial Bi_2O_3 excess content on microstructural and electrical properties of $Bi_4Ti_3O_{12}$ (BIT) ceramics. To vary the Bi_2O_3 content, the ceramics derived from varying amount of initially excess of Bi_2O_3 (3–10 mol%) on the precursor solution were prepared by the polymeric precursor method. Measurements by piezoresponse force microscopy (PFM) reveal that addition of excess bismuth can reduce the strain energy and pin-charged defects and that the perpendicular component of polarization can be switched between two stable states: bright and dark contrast inside and outside of the square region.

II. Experimental

Titanium isopropoxide (97% - Alfa Aesar); bismuth nitrate pentahydrate (100.1% - Mallinckrodt); citric acid (99.5% - Merck); ethlyleneglycol (99.7% - Synth), nitric acid (99.9% - Synth); ethylenediamine (98% - Nuclear) and ammonium hydroxide (99.9% - Qhemis) were used as raw materials. Bismuth and titanium precursor solutions were prepared by adding the raw materials to ethylene glycol and concentrated aqueous citric acid under heating and stirring. The molar ratio of metal : citric acid : ethylene glycol was 1 : 4 : 16. Appropriate quantities of Ti and Bi solutions were mixed and homogeneized by stirring at 90°C for 2 hours. Then the temperature was increased to 130–140°C, yielding a highly viscous polyester resin. Most of the organic material was decomposed by thermal treatment at 300°C for 2 hours. The formed porous product was crushed and heated in an aluminium crucible at 700°C for 4 hours to eliminate residues of organic material. The powders were milled for 4 hours with zirconia balls and isopropyl alcohol with and without excess Bi. The bismuth titanate compositions were designed as BIT, BIT3, BIT5 and BIT10 which corresponds to 0, 3, 5 and 10 mol% of excess Bi_2O_3. The powders were uniaxialy (150 MPa) and isostatically pressed (210 MPa) into pellets. The sintering was performed on pellets packed into covered alumina crucibles, carried out in air at a temperature of 800°C for 1 hour (heating and cooling rate of 10 °C/min).

Raman scattering of powders was performed at room temperature (Fourier transform - RFS 100/S Bruker, excited by a Nd-YAG laser in 1064 nm). The band gap values were obtained using ultraviolet spectroscopy in the visible region curve (UV-vis-NIR Spectrophotometer - Varian Cary 500 X). For Rietveld analyses, X-ray diffraction data were collected with a Rigaku 20-2000 diffractometer under the following experimental conditions: 40 kV, 30 mA, 2θ from 20° to 120°, step size of 0.02°, λCu K_α monocromatized by a graphite crystal, divergence slit of 2 mm, reception slit of 0.6 mm and step time of 10 s. The Rietveld analysis was performed with the Rietveld refinement program DBWS-941 1 [16]. The profile function used was the modified Thompson-Cox-Hasting pseudo-Voigt, in which η (the Lorentzian fraction of the function) varies with the Gauss and Lorentz components of the full width at half maximum.

Bulk densities and weight loss of the sintered pellets were measured by the Archimedes method. The phase formation and crystallinity were studied by X-ray diffractometry (XRD) with Cu Kα radiation using a normal θ-2θ scanning method (Rigaku RINT2000 diffractometer). A scanning electron microscope (SEM) was used to analyze the morphology and shape of the grains (Topcom SM-300).

Dielectric permittivity measurements were performed in HP 4192A LF Mountain View impedancemeter attached to a Flyever oven (FE50RP temperature controller). Silver electrodes for electrical measurements were deposited on the polished surface of sintered pellets by evaporation through a sputtering system. Resistivity was determined by current-voltage in a voltage source (Keitley 237 - USA).

Piezoelectric measurements were carried out using a setup based on an atomic force microscope in a Multimode Scanning Probe Microscope with Nanoscope IV controller (Veeco FPP-100). In our experiments, piezoresponse images were acquired in ambient air by applying a small *ac* voltage with amplitude of 2.5 V (peak to peak) and a frequency of 10 kHz. To apply the external voltage a standard-gold coated Si_3N_4 cantilever with a spring constant of 0.09 N/m was used. The probing tip, with an apex radius of about 20 nm, was in mechanical contact with the uncoated film surface during the measurements. Cantilever vibration was detected using a conventional lock-in technique.

III. Results and discussion

Figure 1 shows the XRD patterns of BIT powders with various amounts of excess Bi_2O_3. All the peaks are indexed by a JCPDS card of BIT (ICSD no. 24735 with a space group of *Fmmm*). Increasing amounts of initial excess Bi_2O_3, leads to a single BIT phase crystallized in the orthorhombic structure [17]. The excess of bismuth forms a solid solution in the BIT lattice having no influence on long distance ordering. The peaks are indicative of a polycrystaline phase with orientation in the *c*-plane and mainly characterized by a higher intense peak (*hkl* - 117). Our XRD results are in agreement with the results reported in the literature [18–21]. The experimental lattice parameter values were calculated using the Rietveld method [16]. We can observe that the polymeric precursor method permits the attainment of BIT powders at a low heat treatment temperature and reduced synthesis time. Moreover, the lattice parameter values obtained by this method presented small variations as compared to the values reported in the literature [22–27]. These differences are related to the preparation method, synthesis conditions (heat treatment temperature, time), lattice distortion and residual stresses in the lattice and/or structural defects. To get more details about crystal structure of BIT system when more bismuth was added, Rietveld analyses of other compositions were performed and the results will be published in a near future.

The BIT system has already been investigated from a fundamental point of view [28]. In the present study, we have adopted the Rietveld refinement technique to investigate the crystal structure of the BIT10 system. Table 1 illustrates the R_{wp}, R_{exp}, and *S* indexes, as well as the lattice parameters (*a*, *b* and *c*) and the unit cell volume (*V*). The phase identification was carried out in the PDF data bank, resulting in an orthorhombic structure type. The structural model (available on the ICSD da-

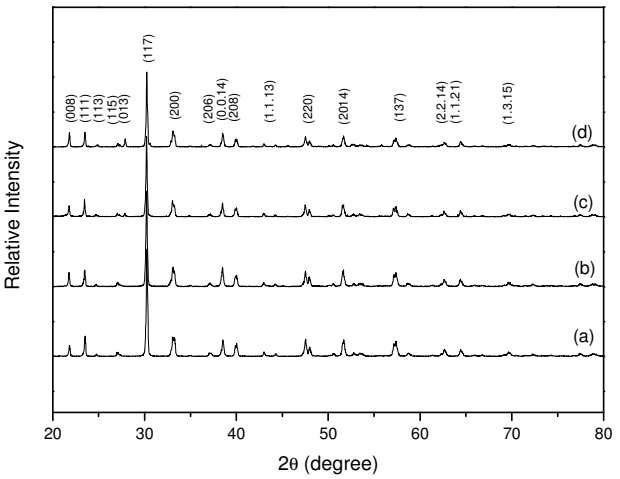

Figure 1. X-ray diffraction at room temperature for: a) BIT, b) BIT3, c) BIT5 and d) BIT10 powders calcined at 700°C for 4 h

Table 1. Refinement Indexes for $Bi_4Ti_3O_{12}$ powders calcined at 700°C for 4 hours with 10 mol% of excess bismuth

Refinement Indexes		Atomic Positions		S_{Occ}		Lattice	
R_{WP} [%]	11.12	A1	0; 0; 0.06722	Bi (A1)	1.00000	*a* [Å]	5.4175
R_{EXP}	7.06	A2	0; 0; 0.21091	Nb (A1)	0.00000	*b* [Å]	5.4403
S	1.57	B1	0; 0; ½	O	0.91700	*c* [Å]	32.7862
		B2	0; 0; 0.37099			*V* [Å^3]	966.30
		O1	¼; ¼; 0			*d* [g/cm^3]	8.02
		O2	¼; ¼; ¼				
		O3	0; 0; 0.43786				
		O4	0; 0; 0.32536				
		O5	¼; ¼; 0.11165				
Perovsquite [mol%]		Stoichiometry				Refinement	
97.5 ± 0.5		$Bi_4Ti_3O_{12}$				$Bi_4Ti_3O_{11.6}$	

tabank) that allows the best fit was the orthorhombic model (ICSD no. 24735 with a space group of *Fmmm*). Quantitative phase analyses for the orthorhombic phase were calculated according to the reference of Young and Wiles [16]. The covalent interaction originating from the strong hybridization between Ti 3d and O 2p orbitals, plays an important role in the structural distortion of the BIT compound. It can be assumed that addition of excess of bismuth improves oxygen ion stability in the lattice because some of the Bi ions in the pseudo-perovskite layers containing Ti–O octahedral were not volatilized. The low *S* values ($S = R_{wp}/R_{exp}$) indicates the good quality of the refinement; the calculated parameters are closer to literature data [29]. Therefore, we can assume that the addition of excess bismuth stabilizes the oxygen vacancies and consequently the structure.

The weight loss and relative density as a function of excess Bi_2O_3 are shown in Fig. 2. It can be seen that the weight loss increases with increasing excess Bi_2O_3 because the low temperature sintering inhibits bismuth oxide volatilization. The relative density measured by the Archimedes method increases with excess Bi_2O_3 reaching around 90% of the theoretical density of BIT, corresponding to 8.038 g/cm^3. This result is not satisfactory from an electrical point of view, since the polarization and dielectric permittivity are dependent on the level of porosity and grains morphology, but it is still a very interesting effect.

UV-vis spectroscopy measurements were evaluated in the BIT powders (see Fig. 3). The maximum absorption was located at around 400 nm with respective band gap values determined from the Kubelka Model [30]. The optical energy band gap is related to the absorbance and to the photon energy by the following equation:

$$h\nu\alpha \propto (h^{o} - E_g^{opt})^2 \quad (1)$$

where α is the absorbance, h is the Planck constant, ν is the frequency and E_g^{opt} is the optical band gap [31]. The obtained values are 3.13, 3.02, 3.03, 3.03 eV, which are similar to the values reported by Wei *et al*. [32] (around

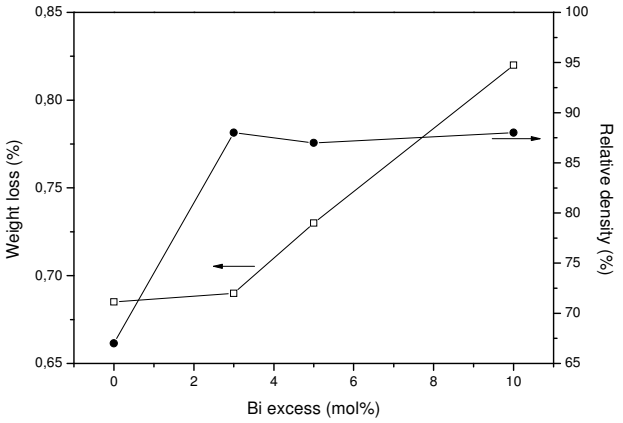

Figure 2. Relative density and weight loss of the sintered pellets versus excess bismuth

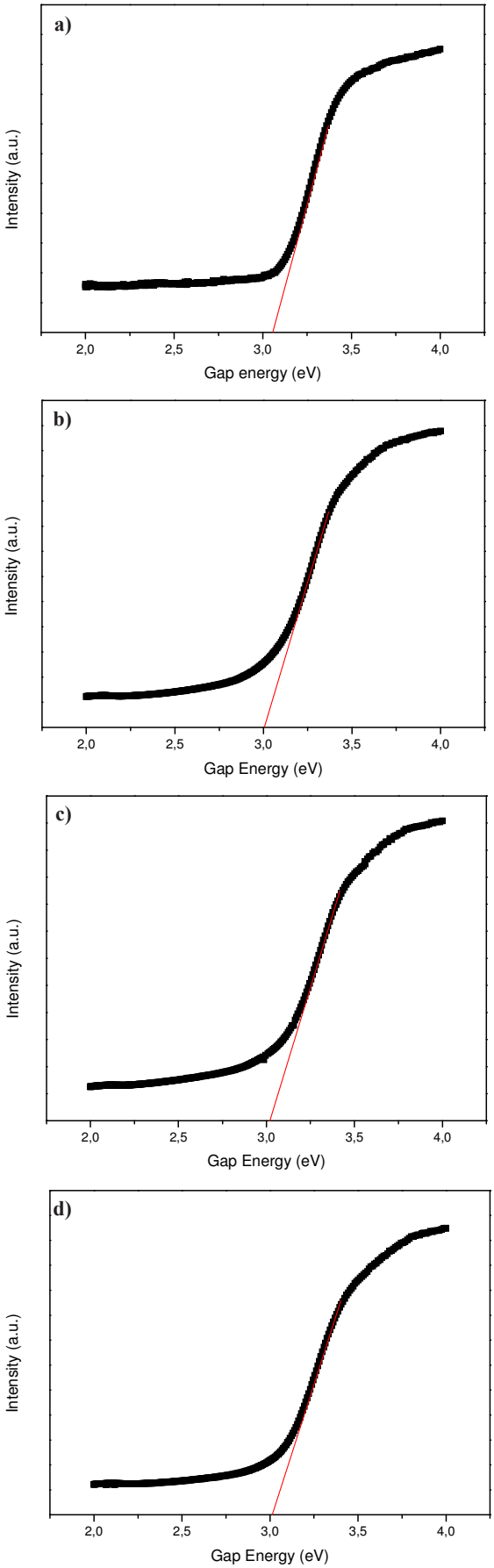

Figure 3. UV-vis absorption spectra at room temperature for: a) BIT, b) BIT3, c) BIT5 and d) BIT10 powders calcined at 700°C for 4 h

3.08 eV). Our BIT powders presented characteristic absorption spectra of ordered or crystalline materials. These results indicate that the exponential optical absorption edge and the optical band gap are controlled by the degree of structural disorder in the BIT lattice. This decrease in the band gap can be ascribed to a reduction of defects in the lattice which decreases the intermediary energy levels due to the reduction of oxygen vacancies located at BO_6 octahedra. The main differences in optical band gaps can be related to the different factors, mainly including: synthesis method, shape (powder, crystal or thin film) and synthesis conditions.

Raman scattering has proven to be a valuable technique to obtain information about local structures within materials. Figure 4 shows the Raman spectra of BIT powders derived from different excess Bi_2O_3 at room temperature. To better denote the peak position, Raman modes are presented in Table 2. The order-disorder degree in the crystal lattice of BIT powders at short and medium distances was investigated. Raman modes located at 96, 119, 189, 223, 266, 315, 450, 536, 615 and 848 cm^{-1} are characteristics of the BIT phase [33]. The modes located under 200 cm^{-1} can be related to vibrations between Bi and O atoms [34]. For BIT10, it is evidently a characteristic mode around 100 cm^{-1} and is probably due to a distortion in the A site caused by the bismuth ion. This distortion into the A site of the perovskite enhances the Jahn-Teller distortion of TiO_6 octahedra. On the other hand, Raman modes located above 200 cm^{-1} are responsible for distortions and vibrations of TiO_6 octahedra. As the content of excess bismuth increases, there is a reduction in the Raman band intensities, (mainly the mode located at 266 cm^{-1}). This is due to the vibrations of Ti-O atoms inside the perovskite layer and to vibrations of Bi-O atoms within the Bi_2O_2 layer [35]. The main bands at 266, 536 and 848 cm^{-1}, originated from TiO_6 octahedra, share a similar excess bismuth behaviour (they reduce its intensity and become broaden with increasing Bi excess). The modes at 230, 268, 328, 530, 563 and 850 cm^{-1} are assigned to stretching and bending vibrations of TiO_6 octahedra because the addition of excess Bi_2O_3 implies a distortion of Bi_2O_2 layers. Raman results are in agreement with XRD data. The appearance of a Raman mode at low-frequency (96 cm^{-1}) is due to the atomic mass of Bi ions which causes Bi displacements in the Bi_2O_2 layer [36]. Raman modes located at 450 and 96 cm^{-1} were evident in BIT10 composition, indicating that 10 mol% of excess bismuth may cause lattice distortions and stoichometric changes. Raman results are in agreement with XRD data, indicating an ordered structure at short and long distances.

The microstructures of the sintered pellets were examined by SEM analyses and are illustrated in Fig. 5. The influence of excess bismuth on the shape and size of the grains was evaluated. The grain size is heterogeneously distributed and presents rod-like form morphology which is different from literature data [37]. BIT presents a porous microstructure with compact region with a very small grain size when compared to ceramics with excess bismuth. The BIT3, BIT5 and BIT10 compositions are dense but pure BIT is prone to form a porous structure with a quite a number of voids which can affect the ferroelectric and dielectric properties of ceramics. All ceramics are stoichiometric, evidencing no losses of Bi_2O_3 during the calcination and sintering process indicating that the initial Bi_2O_3 excess is sufficient to compensate for the bismuth oxide volatilization and fill the Bi vacancy in the lattice. Literature data revealed that some excess of bismuth in the BIT ceramic cannot enter into the lattice. The Bi_2O_3 excess may exist as an impurity phase such as bismuth oxide, which would affect the microstructural and ferroelectric properties of ferroelectric material [38]. The densities of BIT ceramics increase with content of excess bismuth due to the formation of oxygen vacancies originate during the calcinated process of the ceramics and substitution of excess of bismuth. That leads to nega-

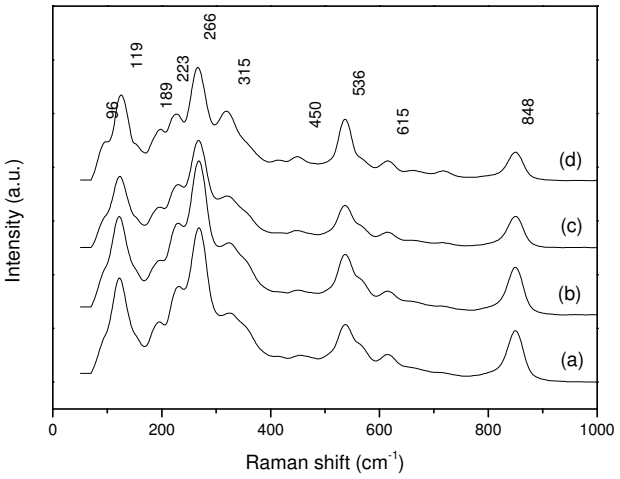

Figure 4. Raman spectra at room temperature for: a) BIT, b) BIT3, c) BIT5 and d) BIT10 powders calcined at 700°C for 4 h

Table 2. Raman modes of $Bi_4Ti_3O_{12}$ powders calcinated at 700°C for 4 hours with several excess bismuth

Compositions	Raman modes [cm^{-1}]
BIT	119, 189, 223, 266, 315, 536, 615, 848
BIT3	119, 189, 223, 266, 315, 536, 615, 848
BIT5	119, 189, 223, 266, 315, 536, 615, 848
BIT10	96, 119, 189, 223, 266, 315, 450, 536, 615, 848

tive charges associated with the presence of negatively charged oxygen trapped at the grain boundary. The negative charge of the oxygen may be caused by charge transference between the metal vacancy and the oxygen, as shown in:

$$V''_m + \tfrac{1}{2}\, O_2^x \rightarrow V^x_m + \tfrac{1}{2}\, O''_2 \quad (2)$$

where O^x, V''_m, V^x_m and O''_2 represent the neutral oxygen ions in their normal position, metal site vacancies doubly negatively charged, neutral metal site vacancies, and oxygen ions doubly negatively charged, respectively.

The leakage current as a function of the electric field reveals a direct relationship to electrical conductivity (Fig. 6). Leakage current is one of the most important properties of BIT because high electrical conductivity makes it difficult to polarize the material and minimize the ferroelectric properties [39]. Considering bismuth oxide volatilization during sintering, it is reasonable to assume that electrical conduction associated with vacancies should occur in BIT, aside from the intrinsic hole conduction. The main conduction mechanism of pure BIT is an electronic *p*-type. The leakage current of samples with excess bismuth was significantly decreased in comparison with BIT. The increase in excess bismuth results in a reduction of conductivity due the improvement of BIT matrix holes. The generation of holes can be represented by the following defect reaction [40]:

$$Bi^{3+} \rightarrow Bi^{(3-x)+} + x\, h^{\cdot} \quad (1)$$

This reaction indicates that holes defects present in BIT are responsible for the leakage current behaviour and consequently the conductivity. Due to the suppression of bismuth oxide volatilization by the addition of excess bismuth the number of carriers associated with vacancy should be remarkably reduced in BIT with excess compositions, indicating a decrease in the leakage current. The addition of excess Bi_2O_3 resulted in a considerable decrease in the leakage current, due to the presence of Bi vacancies (V'''_{Bi}) accompanied by oxy-

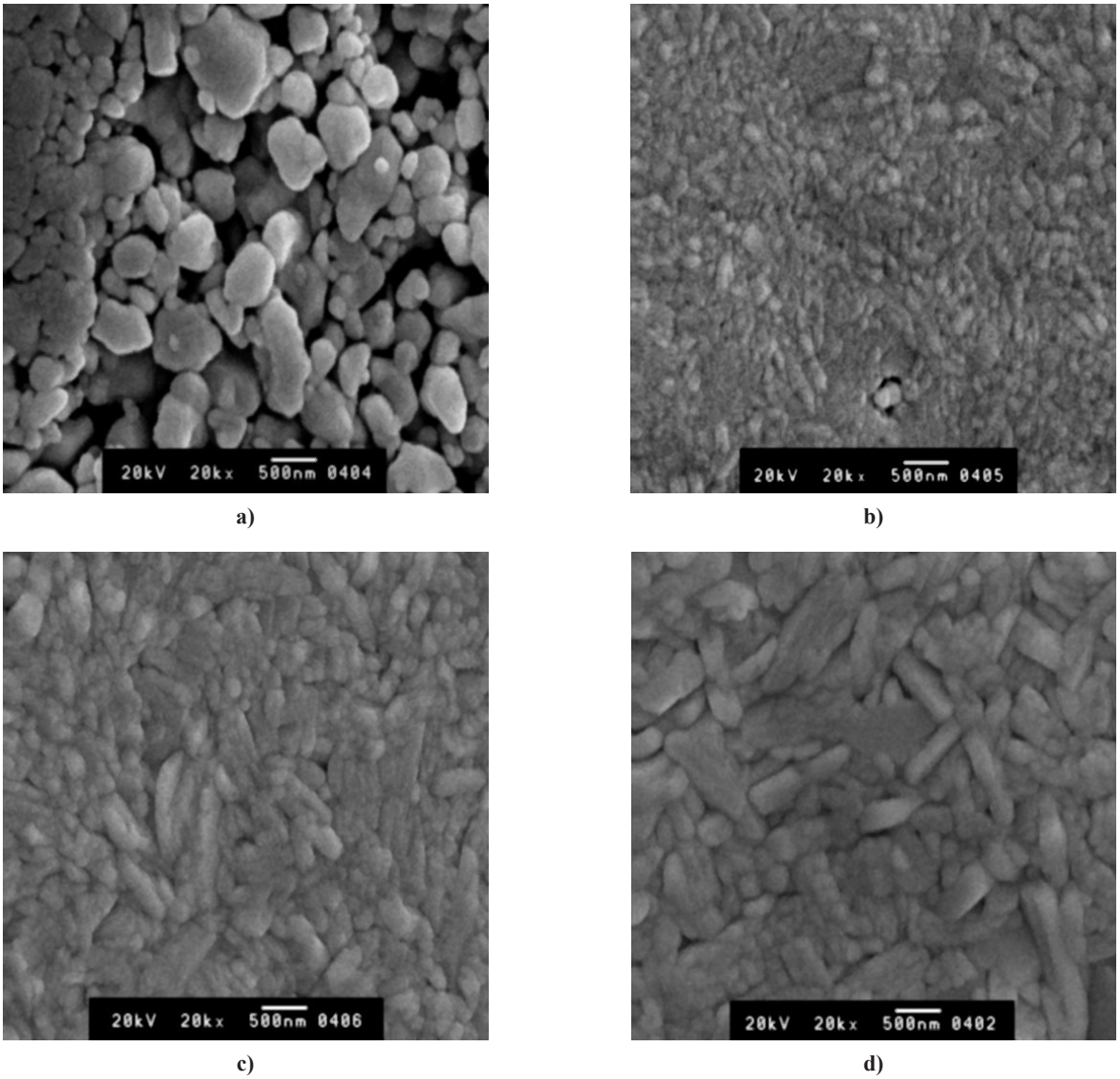

a) **b)** **c)** **d)**

Figure 5. Scanning electronic microscopy for: a) BIT, b) BIT3, c) BIT5 and d) BIT10 ceramics sintered at 800°C for 1 h

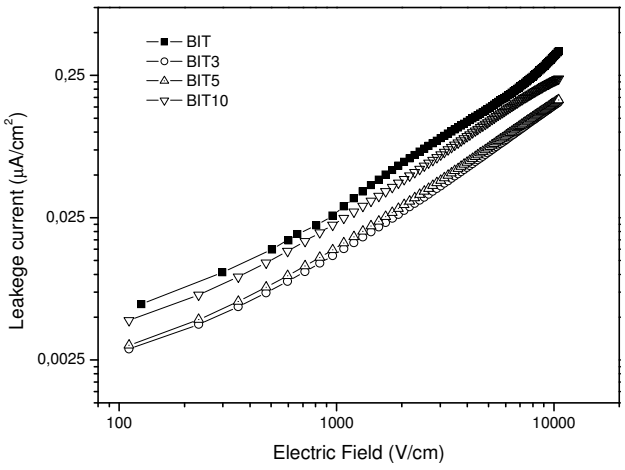

Figure 6. Leakage current behavior as a function of electric field for BIT, BIT3, BIT5 and BIT10 ceramics sintered at 800°C for 1 h

gen vacancies ($V_{\ddot{O}}$). Although the leakage-current properties were improved by excess bismuth, there is a decrease in the V'''_{Bi} and $V_{\ddot{O}}$ density [41]. Also, BIT has rod-like-shaped grains with residual porosity which could have many carrier traps. In the high electric field region, the localized carriers begin to come out of the trap, resulting in a large increase in the current density. A large leakage current was also observed by Cho *et al.* [42], who observed that for BIT films, annealed in a nitrogen atmosphere with a porous microstructure, there are many carrier traps inside it and for higher fields these charges are ejected.

Figure 7 shows the temperature-dependent dielectric permittivity measured at 100 KHz. There are several factors that affect the dielectric permittivity of ferroelectric ceramic samples, including grain size, impurity and concentration of the space charge. As expected, the dielectric permittivity rapidly increases at temperatures above 400°C due to the low electrical conductivity in this region. Below 450°C the dielectric permittivity increases with the addition of excess bismuth. Furthermore, the significantly enhanced dielectric permittivity can be understood as follows: oxygen-vacancy-induced dielectric polarization becomes predominant due to an increased vacancy concentration and inertia of oxygen ions [43]. As the grain becomes larger, an increase in the

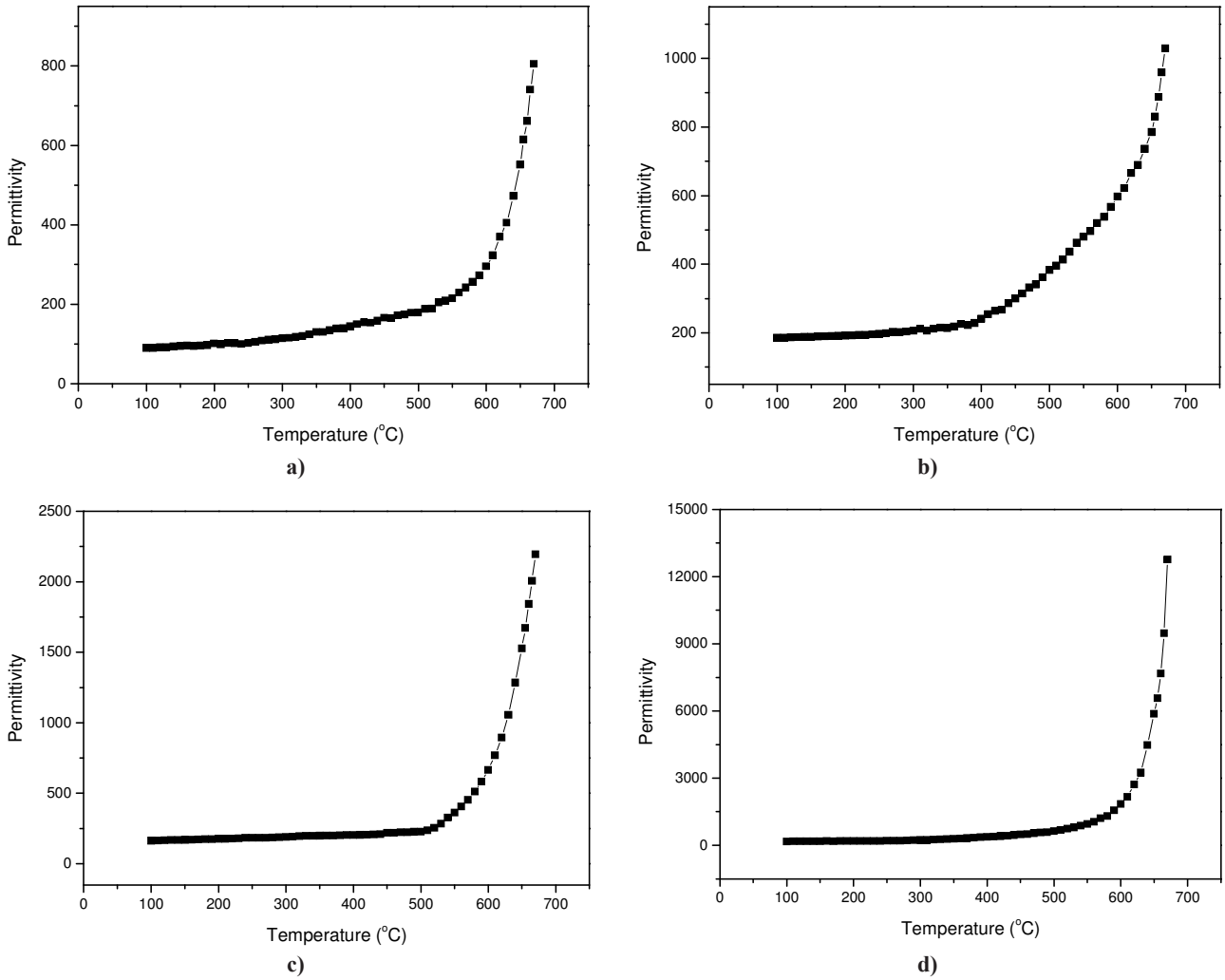

Figure 7. Dielectric permittivity as a function of temperature for: a) BIT, b) BIT3, c) BIT5 and d) BIT10 ceramics sintered at 800°C for 1 h

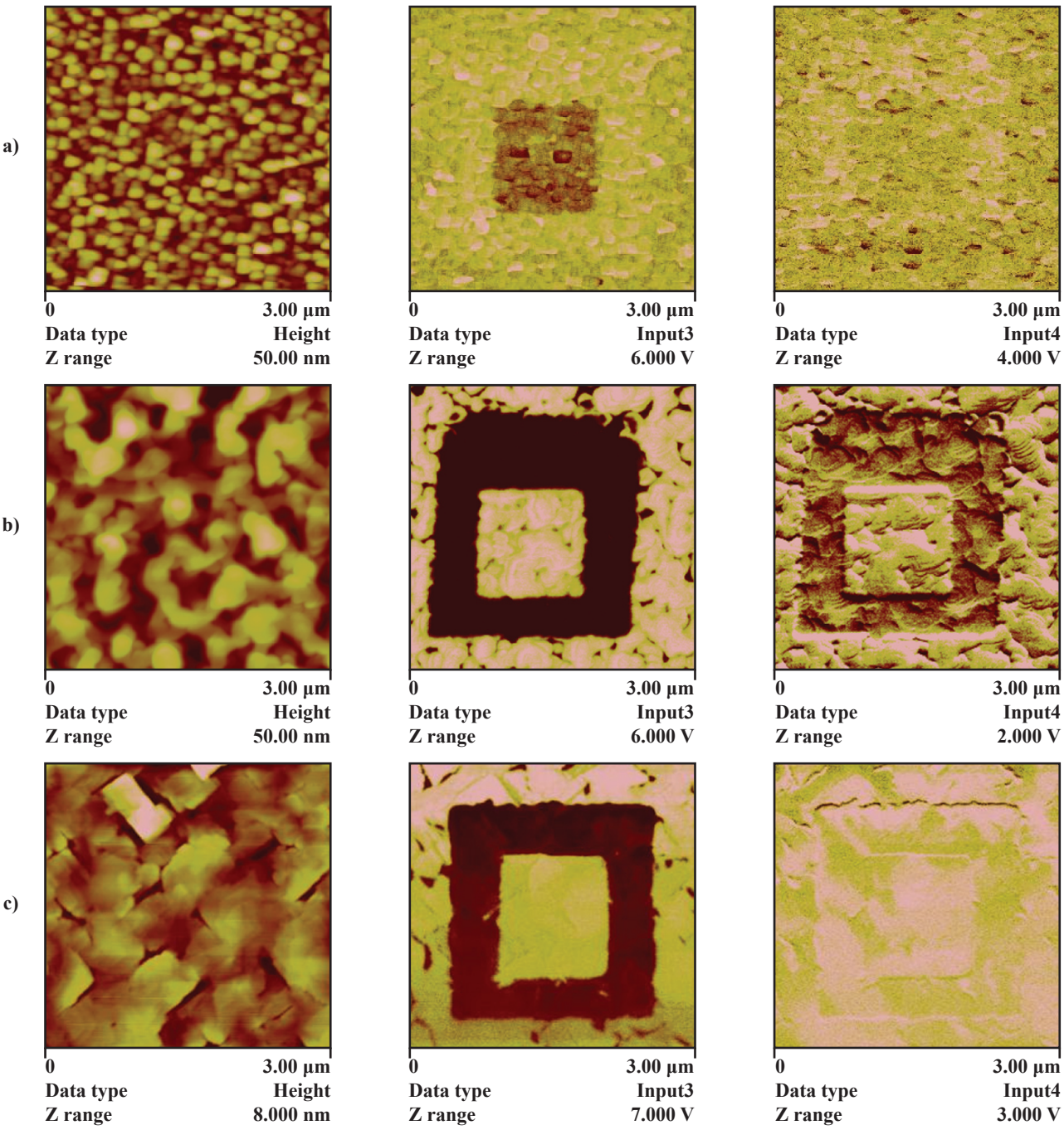

Figure 8. AFM-topography (left), out-of-plane PFM (central) and in-plane PFM (right) images of the pellets sintered at 800°C for 1 h: a) BIT, b) BIT5 and c) BIT10

dielectric permittivity was verified. The incorporation of excess bismuth suppressed the volatilization of bismuth during sintering and reduced the bismuth and oxygen vacancy concentrations in the sintered sample. As a result, the electrical conductivity was significantly reduced, and the polarization was greatly improved. In our study, the main reasons for changes in the dielectric behaviour can be associated with decreased grain size and increased concentration of the space charge. Among all investigated BIT ceramics, the highest dielectric permittivity is shown for the BIT10 sample, where a dielectric permittivity of 12600 was measured at 100 kHz.

To characterize the local ferroelectric properties, ferroelectric domains were polarized and imaged using a commercial AFM equipped with a conducting tip and operating under ambient conditions. To polarize domains, a voltage larger than the coercive voltage of the ferroelectric was applied to the tip while scanning in contact with the sample surface. To read the resulting domain structure, the piezoelectric response was measured. In this technique, the tip is scanned in contact with the sample surface while applying an *ac* voltage smaller than the coercive voltage across the ferroelectric, with the resulting piezoelectric deformation

being detected with a standard lock-in measurement. The out-of-plane (*OP*) and in-plane (*IP*) piezoresponse images of the as-grown sample (after applying a bias of –15 V), on an area of 2 μm × 2 μm, and then an opposite bias of +15 V in the central 1 μm × 1 μm area were measured. BIT, BIT3, BIT5 and BIT10 samples were analyzed. For comparison the topography of the sample was also presented (Fig. 8). The clear regions in the out-of-plane PFM images (Fig. 8) correspond to domains within the polarization vector oriented toward the bottom electrode (hereafter referred to as down polarization, while the dark regions correspond to domains oriented upward (referred to as up polarization). Grains which exhibit no contrast change are associated with zero out-of-plane polarization. A similar behaviour was observed when a positive bias was applied to the ceramic. We noticed that some of the grains exhibit a clear contrast associated with a component of the polarization pointing toward the bottom of the sample. On the other hand, in the in-plane PFM images (Fig. 8) the contrast changes were associated with changes in the in-plane polarization components. In this case, a clear contrast indicates polarization (e.g. in the positive direction of the y-axis) while a dark contrast is the result of in-plane polarization components pointing to the negative part of the y-axis. This result is common for bismuth-layered ferroelectrics, which exhibit a great polarization in the *a*-axis direction, along with a smaller polarization along the *c*-axis and reflects the different orientation of the grains, i.e. the light regions are *c*-axis oriented crystallites. Since the image does not change even for high voltages, it can be concluded that it is impossible to align their polarization vector, so the total polarization in the field direction is always moderate. By changing the polarity of the applied voltage it can easily be demonstrated that the light regions present a polarization vector perpendicular to the sample surface, whereas in dark regions the polarization vector lies in the sample plane. The improvement of piezoelectric response with excess Bi_2O_3 originates from a better polarizability along the *a*-axis, which contributes significantly to the piezoelectric properties of bismuth titanate resulting in a reduction of strain energy and the pinning effect of charged defects. The in-plane images show light-colored grains presenting a polarization vector in the positive y-axis direction and dark grains with exactly opposite polarization. Grains with intermediate contrast do not present overall piezoelectricity, probably due to pinned domains. Therefore, we supposed

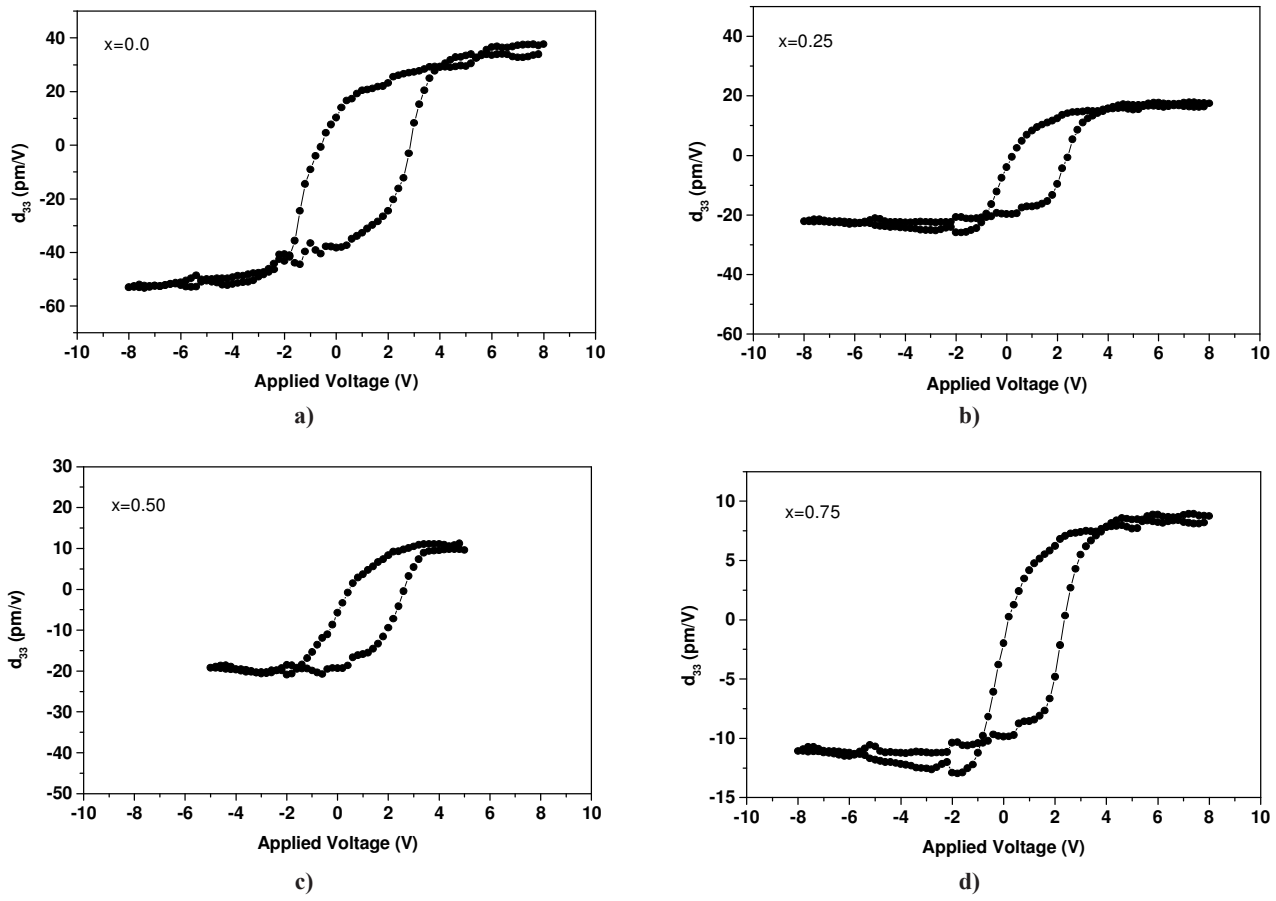

Figure 9. Piezoelectric coefficient as function of voltage for: a) BIT, b) BIT3, c) BIT5 and d) BIT10 ceramics sintered at 800°C for 1 h

that excess Bi_2O_3 is changing the lattice vibration of BIT affecting the piezoelectric properties.

Figure 9 shows the piezoelectric hysteresis loop obtained for the BIT free of excess and with various amounts of excess Bi_2O_3. The hysteresis in the piezoresponse signal is directly associated with the polarization switching and ferroelectric properties of the sample. The maximum d_{33} value of ~45 pm/V is higher for the BIT10 system and approaches the reported value for a BIT single crystal [44]. Here, we point out that it is difficult to compare these values to the piezoelectric coefficients of bulk material since the measurement was performed on a local area that has a relatively intricate field distribution and vibrational modes. Considering the polycrystalline nature of our sample the effective piezoelectric coefficient depends on grain orientation. Therefore, as expected the piezoelectric response changes with increase of bismuth excess due the reduction in the strain energy and the pinning effect of charged defects after doping.

IV. Conclusions

In summary, bismuth titanate ($Bi_4Ti_3O_{12}$, BIT) ceramics derived from different amounts of initial excess Bi_2O_3 were prepared by the polymeric precursor method. An XRD analysis shows that increasing excess Bi_2O_3 single phase BIT powders with an orthorhombic structure were obtained. SEM analyses show grains in the rod-like morphology form; the size decreases with excess bismuth. Due to the suppression of bismuth oxide volatilization by the addition of excess bismuth, there is a reduction in the leakage current and an enhancement of BIT phase dielectric properties. The effective piezoelectric coefficient depends on grain orientation, and excess bismuth was found to effectively induce spontaneous polarization in BIT exhibiting good piezoelectric properties. Due to better electrical properties, BIT with 10 mol% of excess Bi_2O_3 can be considered as a promising composition for application in dynamic random access memories and piezoelectric devices.

Acknowledgements: The authors gratefully acknowledge the financial support agencies in Brazil: FAPESP, CNPq, CAPES.

References

1. B. Aurivillius, "Mixed bismuth oxides with layer lattices: II. Structure of $Bi_4Ti_3O_{12}$", *Ark. Kemi* **1** (1949) 499–512.
2. A.V. Murugan, S.C. Navale, V. Ravi, "Preparation of nanocrystalline ferroelectric $BaBi_4Ti_4O_{15}$ by Pechini method", *Mater. Lett.*, **60** [8] (2006) 1023–1025.
3. E.C. Subbarao, "A family of ferroelectric bismuth compounds", *J. Phys. Chem. Solids*, **23** [6] (1962) 665–676.
4. Y. Noguchi, M. Miyayama, "Large remanent polarization of vanadium-doped $Bi_4Ti_3O_{12}$", *Appl. Phys. Lett.*, **78** [13] (2001) 1903–1905.
5. X.L. Zhong, J.B. Wang, S.X. Yang, Y.C. Zhou. "Dependence of excess bismuth content in precursor sols on ferroelectric and dielectric properties of $Bi_{3.25}La_{0.75}Ti_3O_{12}$ thin films fabricated by chemical solution deposition", *Appl. Surf. Sci*., **253** [2] (2006) 417–420.
6. J.K. Lee, B. Park, K.S. Hong, "Effect of excess Bi_2O_3 on the ferroelectric properties of $SrBi_2Ta_2O_9$ ceramics", *J. Appl. Phys.*, **88** [5] (2000) 2825–2829.
7. A.Z. Simões, G.C.C. da Costa, M.A. Ramirez, J.A. Varela, E. Longo, "Effect of the excess of bismuth on the morphology and properties of the $BaBi_2Ta_2O_9$ ceramics", *Mater. Lett*., **59** [6] (2005) 656–661.
8. A.Z. Simões, E.C. Aguiar, A. Ries, E. Longo, J.A. Varela, "Niobium doped $Bi_4Ti_3O_{12}$ ceramics obtained by the polymeric precursor method", *Mater. Lett*., **61** [2] (2007) 588–591.
9. M. Villegas, A.C. Caballero, C. Moure, P. Duran, J.F. Fernandez, "Low-temperature sintering and electrical properties of chemically W-doped $Bi_4Ti_3O_{12}$ ceramics", *J. Eur. Ceram. Soc.*, **19** [6-7] (1999) 1183–1186.
10. M. Villegas, A.C. Caballero, C. Moure, P. Duran, J.F. Fernandez, "Factors affecting the electrical conductivity of donor-doped $Bi_4Ti_3O_{12}$ piezoelectric ceramics". *J. Am. Ceram. Soc.*, **82** [9] (1999) 2411–2419.
11. M. Villegas, T. Jardiel, A.C. Caballero, J.F. Fernández, "Electrical properties of bismuth titanate based ceramics with secondary phases", *J. Electroceram.*, **13** [1-3] (2004) 543–548.
12. C. Jovalekic, M. Pavlovic, P. Osmokrovic, L. Atanasoska, "X-ray photoelectron spectroscopy study of $Bi_4Ti_3O_{12}$ ferroelectric ceramics", *Appl. Phys. Lett.*, **72** [9] (1998) 1051–1054.
13. M.P. Pechini, "Method of preparing lead and alkaline earth titanates and niobates and coating method using the same to form a capacitor", *US Patent 3330697*, 11 July, 1967.
14. K.T. Kim, C.I. Kim, "Effect of bismuth excess on the crystallization of $Bi_{3.25}La_{0.75}Ti_3O_{12}$ thin films on Pt/Ti/SiO_2/Si substrates", *Microelectron. Eng.*, **71** [3-4] (2004) 266–271.
15. J.L. Lin, T.L. Chang, W.T. Lin, "Effects of excess Bi concentration, buffered Bi_2O_3 layer, and Ta doping on the orientation and ferroelectricity of chemical-solution-deposited $Bi_{3.25}La_{0.75}Ti_3O_{12}$ films", *J. Electron. Mater.*, **33** [10] (2004) 1248–1252.
16. R.A. Young, A. Sakthivel, T.S. Moss, C.O. Paiva-Santos, "*DBWS*-9411 - an upgrade of the *DBWS**.* programs for Rietveld refinement with PC and mainframe computers", *J. Appl. Cryst.*, **28** [3] (1995) 366–367.
17. JCPDS - ICSD 024735, (1997).
18. B.D. Stojanovic, A.Z. Simões, C.O. Paiva-Santos, C. Quinelato, E. Longo, J.A. Varela, "Effect of processing route on the phase formation and properties of $Bi_4Ti_3O_{12}$ ceramics", *Ceram. Int.*, **32** [6] (2006) 707–712.
19. Y. Kan, P. Wang, Y. Li, Y.B. Cheng, D. Yan, "Low-temperature sintering of $Bi_4Ti_3O_{12}$ derived from a co-precipitation method", *Mater. Lett.*, **56** [6] (2002) 910–914.

20. M.E. Mendoza, F. Donado, J.L. Carrillo, "Synthesis and characterization of micrometric ceramic powders for electro-rheological fluids", *J. Phys. Chem. Solids*, **64** [11] (2003) 2157–2161.
21. W.K. Chia, C.F. Yang, Y.C. Chen, "The effect of Bi_2O_3 compensation during thermal treatment on the crystalline and electrical characteristics of bismuth titanate thin films", *Ceram. Int.*, **34** [2] (2008) 379–384.
22. J.F. Dorrian, R.E. Newnham, K.K. Smith, "Crystal structure of $Bi_4Ti_3O_{12}$", *Ferroelectrics*, **3** [1] (1971) 17–27.
23. T. Rentschler, "Substitution of lead into the bismuth oxide layers of the N = 2- and N = 3-aurtvillius phases", *Mater. Res. Bull.*, **32** [3] (1997) 351–369.
24. A.Z. Simões, B.D. Stojanovic, M.A. Ramirez, A.A. Cavalheiro, E. Longo, J.A. Varela, "Lanthanum-doped $Bi_4Ti_3O_{12}$ prepared by the soft chemical method: Rietveld analysis and piezoelectric properties", *Ceram. Int.*, **34** [2] (2008) 257–261.
25. M. Zdujic, D. Poleti, C. Jovalekic, L. Karanovic, "The evolution of structure induced by intensive milling in the system $2Bi_2O_3{\cdot}3TiO_2$", *J. Non-Cryst. Solids*, **352** [28-29] (2006) 3058–3068.
26. K.R. Zhu, M.S. Zhang, Y. Deng, J.X. Zhou, Z. Yin, "Finite-size effects of lattice structure and soft mode in bismuth titanate nanocrystals", *Solid State Commun.*, **145** [9-10] (2008) 456–460.
27. M.K. Jeon, Y.I. Kim, S.H. Nahm, J.M. Sohn, C.H. Jung, S.I.Woo, "Crystal structure and spontaneous polarization of $Bi_{4-x}Nd_xTi_3O_{12}$ studied by using neutron powder diffraction data", *J. Phys. D*, **40** [15] (2007) 4647–4652.
28. J.F. Scott, C.A. Paz De Araujo, B.M. Melnick, "Loss mechanisms in fine-grained ferroelectric ceramic thin films for ULSI memories (DRAMs)", *J. Alloys Compd.*, **211-212** (1994) 451–454.
29. S. Luo, Y. Noguchia, M. Miyayamab, T. Kudo, "Rietveld analysis and dielectric properties of Bi_2WO_6-$Bi_4Ti_3O_{12}$ ferroelectric system", *Mater. Res. Bull.*, **36** [3-4] (2001) 531–540.
30. P. Kubelka, F. Munk, "Ein beitrag zur optik des farbanstriche", *Zeitschrift für Technische Physik,* **12** (1931) 593–601.
31. D.L. Wood, J. Tauc, "Weak absorption tails in amorphous semiconductors", *Phys. Rev. B.*, **5** (1972) 3144–3151.
32. W.F. Yao, X.H. Xu, H.W., J.T. Zhou, X.N. Yang, Y. Zhang, S.X. Shang, B.B. Huang, "Photocatalytic property of perovskite bismuth titanate", *Appl. Catal. B-Environ.*, **52** [2] (2004) 109–116.
33. H. Idink, V. Srikanth, W.B. White, E.C. Subbarao, "Raman study of low temperature phase transitions in bismuth titanate $Bi_4Ti_3O_{12}$", *J. Appl. Phys.*, **76** [3] (1994) 1819–1824.
34. Z.C. Ling, H.R. Xia, W.L. Liu, H. Han, X.Q. Wang, S.Q. Sun, D.G. Ran, L.L. Yu, "Lattice vibration of bismuth titanate nanocrystals prepared by metalorganic decomposition", *Mater. Sci. Eng. B*, **128** [1-3] (2006) 156–160.
35. P. Durán, F. Capel, C. Moure, M. Villegas, J.F. Fernandez, J. Tartaj, A.C. Caballero, "Processing and dielectric properties of the mixed-layer bismuth titanate niobate $Bi_7Ti_4NbO_{21}$ by the metal-organic precursor synthesis method", *J. Eur. Ceram. Soc.*, **21** [1] (2001) 1–8.
36. P.R. Graves, G. Hua, S. Myhra, J.G. Thompson, "The Raman modes of the Aurivillius phases: Temperature and polarization dependence", *J. Solid State Chem.*, **114** [1] (1995) 112–122.
37. Z.S. Macedo, C.R. Ferrari, A.C. Hernandes, "Impedance spectroscopy of $Bi_4Ti_3O_{12}$ ceramic produced by self-propagating high-temperature synthesis technique", *J. Eur. Ceram. Soc.*, **24** [9] (2004) 2567–2574.
38. H. Watanabe, T. Mihara, H. Yoshimori, C.A. Paz de Araujo, "Preparation of ferroelectric thin films of bismuth layer structured compounds", *Jpn. J. Appl. Phys.*, **34** (1995) 5240–5244.
39. Y.N. Kan, G.P. Zhang, P.L Wang, Y.B. Cheng, "Preparation and properties of neodymium-modified bismuth titanate ceramics", *J. Eur. Ceram. Soc.*, **28** [8] (2008) 1641–1647.
40. Z.Y. Zhou, X.L. Dong, H.X. Yan, H. Chen, C. Mao, "Doping effects on the electrical conductivity of bismuth layered Bi_3TiNbO_9-based ceramics", *J. Appl. Phys.*, **100** [4] (2006) 044112(1-5).
41. H. Yan, C. Li, J. Zhou, W. Zhu, L. He, Y. Song, Y. Yu, "Influence of sintering temperature on the properties of high T_c bismuth layer structure ceramics", *Mater. Sci. Eng. B.*, **88** [1] (2002) 62–67.
42. H.J. Cho, W. Jo, T.W. Noh, "Leakage current behaviors in rapid thermal annealed $Bi_4Ti_3O_{12}$ thin films", *Appl. Phys. Lett.*, **65** [12] (1994) 1525–1527.
43. Y.J. Qi, X. Xiao, C.J. Lu, X.Y. Mao, X.B. Chen, "Microstructural, ferroelectric, and dielectric properties of $Bi_{3.15}Nd_{0.85}Ti_3O_{12}$ ceramics", *J. Appl. Phys.*, **98** [9] (2005) 094101(1-5).
44. U. Robels, J.H. Calderwood, G. Arlt, "Coercive and switching fields in ferroelectric ceramics", *Appl. Phys. Lett.*, **81** [14] (1995) 2605–2607.